American Journal of Polymer Science 2022, 11(1): 7-17
DOI: 10.5923/j.ajps.20221101.02

Synthesis, Characterization, and Use of the Dimer of (Nitrato-κ^2 O, O′) Bis (2-(2,4-dinitrobenzyl) Pyridine κ-N) Silver(I) for the Decoration of Polyanilines with Metallic Silver

Jose Medina, Jaclyn McCasland, Jordan McBride, Roch Chan-Yu-King*

University of Science and Arts of Oklahoma, Science Division, Grand Avenue and 17th Street, Chickasha, OK, USA

Abstract The reaction of the photochromic compound, 2-(2, 4-dinitrobenzyl) pyridine, with $AgNO_3$ in methanol yields a coordination product that crystallizes out as the dimer of (Nitrato-κ^2 O, O′) bis (2-(2,4-dinitrobenzyl) pyridine κ-N) silver (I). The organosilver is characterized by ^{1}H-, ^{13}C-NMR, HRMS, elemental analysis, cyclic voltammetry and X-Ray crystallography. On exposure to sun light, the dimer reveals to be devoid of photochromism. However, it can be used to decorate polyanilines (PANI) with metallic silver in a solventless/heterogeneous medium at high temperature or under homogenous condition in NMP solvent at room temperature. Upon decoration, the PANI-Ag composites are analysed via SEM, EDS, UV-Vis and IR. Four-probe measurements of the silver coated polyanilines provide electrical conductivities higher than those of the corresponding silver free parent PANI.

Keywords X-Ray crystallography and ORTEP drawing of the dimer of (Nitrato-κ^2 O, O′) bis (2-(2,4-dinitrobenzyl) pyridine κ-N) silver (I), Thermal/solid state or room temperature post-polymerization decoration of polyanilines with an organosilver (I) coordination compound, Derivative of 2-(2, 4-dinitrobenzyl) pyridine, Band gap of polyaniline-silver composites

1. Introduction

Among the organic photochromic compounds, 2-(2, 4-dinitrobenzyl) pyridine (DNBP) is one of the most investigated [1]. When kept in the dark, this compound is sandy brown in colour which turns into deep blue on exposure to UV/sun light. The mechanism of this reversible photochromic reaction involves the formation of two tautomeric structures. They are generated through an initial intramolecular deprotonation of an acidic benzylic hydrogen by an oxygen of the NO_2 group (Fig. 1) leading to the less stable "OH" tautomer which eventually rearranges to the more stable "NH" intermediate [2]. However, the potential participation of the N-pyridyl atom in photochromism (upon the formation of the tautomers), via an inter or intramolecular charge transfer to the electrophilic dinitrated benzylic ring has not been investigated. In addition, an inhibition of photochromism, through complexation of the N-atom with a transition metal cation has not been addressed. It is well documented that pyridine and its derivatives are often used as ligands for the complexation of transition metal cations in the formation of coordination compounds and the lone pair of nitrogen, in some instances, can transfer its charge to an oxidizing receptor [3]. To gain insight into the above-mentioned potential role of the N-pyridyl atom in charge transfer processes, we have reacted DNBP with silver nitrate and have unexepectedly isolated the dimer of (Nitrato-κ^2 *O, O′*) bis (2-(2,4-dinitrobenzyl) pyridine κ-*N*) silver(I) whose structure is shown in Fig. 2.

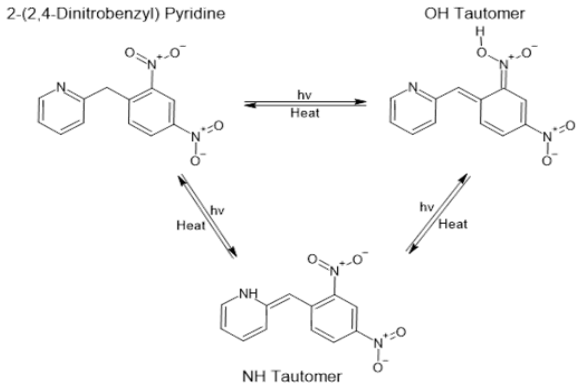

Figure 1. Sun light induced tautomerism in 2-(2,4-dinitrobenzyl) pyridine resulting in photochromism

* Corresponding author:
rchanyuking@usao.edu (Roch Chan-Yu-King)
Received: May 28, 2022; Accepted: Jun. 13, 2022; Published: Jun. 29, 2022
Published online at http://journal.sapub.org/ajps

2. X-Ray Structure of the Dimer

The dimer structure was determined by X-Ray crystallography (details of the crystallographic data on bond lengths, angles, H-bonds are attached in a separate file).

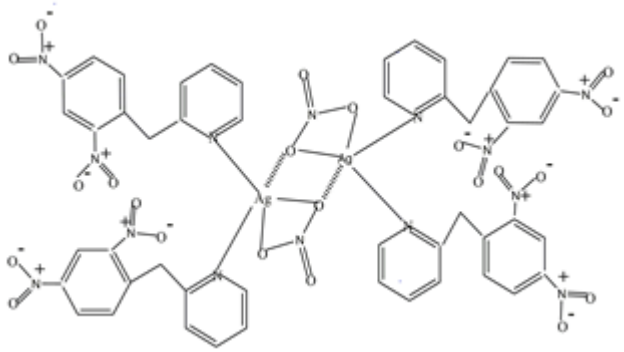

Figure 2. Structure of the dimer of (Nitrato-κ ^{2} *O, O′*) bis (2-(2,4-dinitrobenzyl) pyridine κ-*N*) silver(I). The dotted lines indicate bridges that bond the two monomers

A brief description of the multidimensional structure of the dimer is as follows: Fig. 3 (ORTEP view) shows two individual Ag(I) containing monomers with the bridging bonds left out for clarity. Each Ag(I) center (blue atom) adopts a highly distorted tetrahedron geometry and is bonded to two N-atoms (green atoms) from the DNBP ligands and two O-atoms (red atoms) from a bidentate (NO_3^-) ligand. Fig. 4 (ORTEP view) features the bridges (Ag1-O22 and Ag2-O21) linking the two monomers. The binuclear dimer is rather unique in that each metallic center participates in the formation of a relatively small (Ag1-O22-Ag2-O21) tetracyclic (parallelogram-like) ring in which two trivalently coordinated O-atoms (O22 and O21) are found. A rare but similar type of structure has been reported by Bowmaker et al. in a quinoline Ag(I) nitrate complex [4].

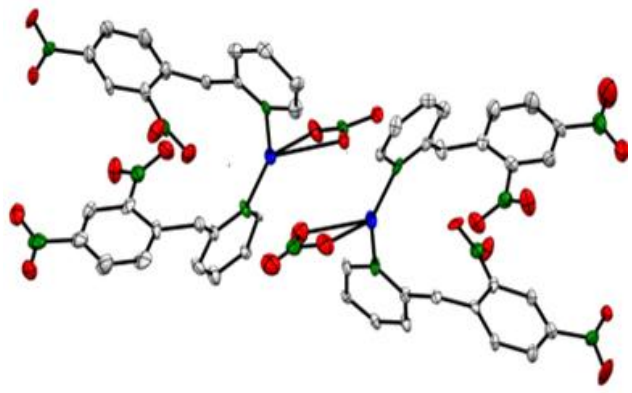

Figure 3. ORTEP view of two monomers of (Nitrato-κ ^{2} *O, O′*) bis (2-(2,4-dinitrobenzyl) pyridine κ-*N*) silver(I). Bridging bonds are not shown

The ORTEP images show two pairs of translated/ displaced DNBP ligands, one of which contains the N_1 B and N_1 D atoms and the other bears the N_1 A and N_1 C atoms. The members of each pair are almost mirror images of each other with their corresponding atoms quasi "diametrically opposed" to the center of the tetracyclic [Ag1-O22-Ag2-O21] ring. The latter observation can also be made for the atoms of rings [(N12-O22-Ag2-O12) and (N11-O21-Ag1-O11)]. The presence of intra and intermolecular hydrogen bonds (H-bonds) have been described in the crystalline structure of the photochromic DNBP molecule with the shortest intra- and intermolecular bond length values of 2.40 Å and 2.60 Å , respectively [5]. Here, the H-bonds from the (acidic) benzyllic hydrogens to the oxygens of NO_2 or NO_3 groups help re-enforce the stability of the dimer. For example, most intramolecular H-bond lengths involving the benzylic hydrogens and the oxygens of NO_2 are below 2.40 Å (with 2.28 Å as the shortest H-bond).

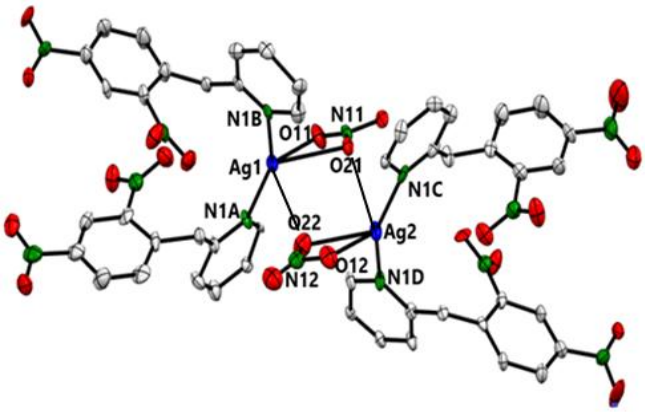

Figure 4. ORTEP view of the dimer featuring bridging bonds (Ag1-O22 and Ag2-O21). C-atoms are in grey, O-atoms in red, and H-atoms are left out

3. Experimental Section

3.1. Synthesis of the Dimer

The DNBP ligand was prepared according to the procedure of Zaccek [6]. It was recrystallized and then reacted with silver nitrate according to the following procedure: a solution of 0.17g (1.00 mmol) of silver nitrate in 7.00 ml methanol was added dropwise to a solution of 0.26 g (1.00 mmol) of DNBP in 6.40 ml methanol. The resulting mixture was stirred at room temperature for 3h after which time it was left undisturbed. The solvent was allowed to partially evaporate for several days resulting in the formation of yellowish crystals which were collected and recrystallized in methanol. The product was filtered, washed with cold hexanes, and then vacuum dried to provide 0.280g (81% yield) of dimer. The yield is based on the amount of ligand as the limiting reactant in a reaction of a 1/2 stoichiometric (metal/ligand) ratio. Elemental analysis (Micro Analysis, Inc.) calculated for $C_{48}H_{36}Ag_2N_{14}O_{22}$ (1376.64): C 41.88%, H 2.64%, N 14.24%; Found: C 41.88%, H 2.60%, N 14.16.

3.2. Spectral Analyses of the Dimer

a) High resolution NMR data are collected with a Varian 300 MHZ broad band Gemini spectrometer:

^{13}C-NMR (DMSO-d_6), δ (ppm): 40.36 (sp^3 C) and

aromatic sp^2 C's: 120.01, 122.19, 123.67, 127.41, 134.60, 137.50, 140.36, 146.39, 148.8, 149.48, 157.37.

^{1}H-NMR (DMSO-d_6), δ (ppm): 4.63 (s, CH_2), 7.29 (m, 1H), 7.35 (d, J=7.9Hz, 1H), 7.81 (m, 2H), 8.44 (m, 1H), 8.50 (dd, J=8.2 Hz, J= 2.2 Hz, 1H), 8.76 (d, J=2.5 Hz, 1H). Both ^{13}C- and ^{1}H-NMR spectra resemble those of the DNBP molecule [7] except the ligand peaks associated with the dimer are all slightly shifted downfiled due to their complexation with the Ag(I) ion.

b) FTIR spectra (400-4000 cm $^{-1}$ range) and UV-Vis (300-900 nm range) of the parent PANI or its polymer-silver composites are recorded with the use of a Nicolet iS10 (Thermoscientific Corporation) and UV-2550 spectrometers (Shimadzu Co.), respectively.

FTIR of the dimer (KBr pellet, cm^{-1}): 3109.15(=C-H stretching), 3079.96 (=C-H stretching), 2923.55 (C-H stretching), 1603.47 (C=C stretching), 1568.47, 1525.87 (NO_2 stretching), 1479.59, 1439.83, 1350.62 (stretching of NO_3^-), 1302.00 (stretching of NO_3^-), 1150.97, 1097.37, 1066.75, 1036.99, 1015.51, 913.50, 853.41(C-H bending), 836.56 (C-H bending), 819.68 (C-H bending), 807.93, 770.81, 740.88, 728.61, 723.07, 686.46, 650.61, 639.66, 611.27.

c) High resolution mass spectral data were obtained with a Bruker 15T FT-ICR instrument. ESI-MS (DMSO solvent).

Keeping in mind that Ag has two major isotopes whose natural abundances are almost in a 1:1 ratio, the two most intense peaks observed in the spectrum belong to the monomeric cation with m/z of 625.341 [M^+] and 627.341 [M^+ + 2]. Other significant peaks have m/z of 365.963 [M^+ - (one ligand)], 367.962 [(M^+ + 2) - one ligand], 260.056 [(one ligand) + H]$^+$,166.946 [dinitrophenyl]$^+$ and 164.946 [dinitrophenyl –(2 H's)]$^+$. The absence of any significant size/detectable dimer molecular ion peak is either due to its high instability under the energy intense mass spectrometry (MS) condition or prior to MS analysis, the dimer would have dissociated readily when dissolved in the polar DMSO solvent. Thus, only the monomeric ions and their fragmented peaks were observed.

3.3. Melting Point of the Dimer

On exposure to sunlight for extending periods, the dimer did not exhibit photochromism. However, when heated, it melted at 126-128℃ producing a yellowish melt at first followed by the gradual formation of spherical, lustrous silver particles around 135-138℃ (inset in Fig. 5).

3.4. Cyclic Voltammetry of the Dimer

The electrochemical data were collected using a CH-instrument (CHI 760D) potentiostat equipped with Electrochemical Analyzer software (version 15.03). The reference electrode is Ag/AgCl. The counter electrode is platinum based with surface area of 1x1 cm^2. The dimer (3mg) was deposited on carbon cloth (1x1 cm^2) functioning as the working electrode. The electrolyte and scan rate are 1M Na_2SO_4 and 10 mV/s, respectively. The cyclic voltammogram (Fig. 5) shows an oxidation and reduction peaks of silver at 0.522V and 0.292V, respectively.

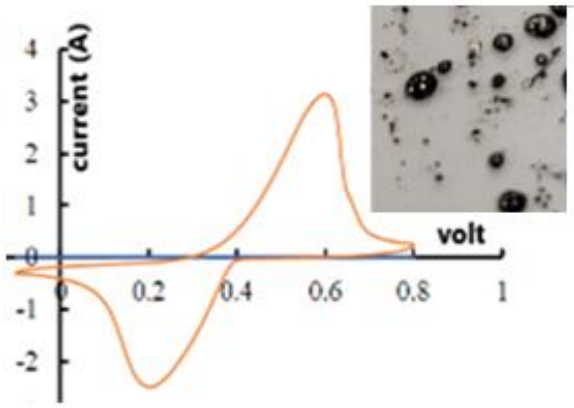

Figure 5. Cyclic voltammogram of the dimer (scan rate 10mV/s). Inset: photograph of metallic silver particles formed upon heating the dimer

3.5. Analyses of the Parent Polymer and Its Composites

a) Electrical conductivity

The conductivity of the parent ES and its silver composites was measured on pelletized powder, which was compressed with a hydraulic press at 700 MPa, resulting in a circular pellet of 13 mm in diameter with a thickness of about 0.95 mm. The pellets were then connected to a four point-probe device which is linked to a Lakeshore 120CS DC microcurrent source coupled to an auto ranging multimeter 175A (Keithley/Tektronix Co.) The current is passed through two adjacent contacts and the resulting voltage recorded. The electrical measurements were conducted on both sides of the pellet. The conductivities are determined via the Van Der Pauw method [8] and their values averaged out.

b) Morphology

Surface morphological characteristics of PANI composites are obtained via a SEM instrument (Zeiss Neon EsB operating at 5 KV) which is connected to an energy dispersive X-ray spectrometer (EDS) operating at 10-15 KV. Prior to SEM analyses, the composites were briefly sonicated in water and a sample of the suspension was retrieved via pipet and then air dried.

3.6. Typical Procedures for the Preparation of the Parent ES and EB

Into a 250-mL beaker, containing a magnetic stir bar, was placed a solution of 1.56g (16.0 mmol) freshy distilled aniline in 120 mL 1M HCl. To this stirred solution was added 4mg of SWNT used as template to guide PANI nanofiber growth [9], [10]. Then a solution of 0.73g (3.19 mmol) of ammonium peroxydisulfate (APS) in 80 mL 1M HCl was added to the anilinium chloride solution in small portions. The resulting mixture was stirred overnight, suction filtered to yield a deep green precipitate which was washed with

copious amounts of water, and then acetone until the washings became colourless. The ES was high vacuum dried for 5 h at 50℃. To prepare the corresponding EB, the as-prepared/dried ES was placed in a 1L volumetric flask containing 0.10M NH_3 (aq) The mixture was stirred overnight, and suction filtered. The cake was washed with abundant amounts of water, and then acetone. The deep blue EB was collected and then high vacuum dried for 6 h at 50℃.

3.7. Typical Procedures for the Decoration of EB and Its Post Protonic Doping to ES-Ag (6%) Composite

All experiments were repeated at least twice. It is worth noting that in this work the post polymerization metal decoration of the PANI starts invariably with EB. Had ES and the dimer been used as reagents, there could be potential precipitation of AgCl since the chloride ions from the ES and the silver (I) ion in the dimer could combine to form the precipitate.

a) Under thermal condition in a heterogenous medium.

Into a mortar were placed 200 mg of EB and 81 mg dimer of which 12.7 mg is Ag (the dimer contributes a theoretical 6% Ag by mass in the final composite). The mixture was pulverized in the mortar with a pestle. The powder was transferred into a test tube and then heated in a sand bath up to 145℃ at which point the heat bath was removed. The mixture was allowed to cool and then diluted in 100 mL DI water with stirring. The top portion of the liquid supernatant was discarded, the remaining mixture centrifuged and the water was discarded. This step was repeated three more times. Acetone was then added to the solid residue under stirring. The mixture was centrifuged, and the solvent was discarded. Additional washings with acetone were repeated until the solvent became colourless. The resulting solid, obtained after centrifugation, was dried under high vacuum at 60℃ for 4h. To convert the EB-Ag to the conducting ES-Ag, the composite was placed in 500 mL 1M HCl (aq) and the suspension was stirred overnight. The mixture was suction filtered, sequentially washed with water and acetone and then dried in high vacuum for 6h at 60℃.

b) At room temperature in a homogeneous medium.

Into a 50 ml Erlenmeyer flask containing 6.10g NMP was added, in small portions with stirring (over the course of 60 min) 200mg of pulverized EB. The mixture was stirred for 4 hours and a solution of 81 mg of dimer in 0.20g NMP was added in small volumes over a 30-min period. The resulting solution was further stirred overnight after which time, it was transferred to a beaker containing 300 ml DI water. This mixture was allowed to settle and about 2/3 of the top deep blue supernatant was discarded. The remaining suspension was centrifuged, and the solid residue was sequentially washed and centrifuged two more times with DI water. It was then repeatedly washed with acetone and centrifuged until the solvent became colourless. The composite was dried in high vacuum for 6 h (50℃). The conversion of the isolated EB-Ag to ES-Ag composite was conducted in the same manner as described above.

4. The Common Oxidation States of PANI

Polyaniline (PANI) is one of the most studied, environmentally stable, and intrinsically conducting polymers. The three commonly cited oxidation states of PANI are Pernigraniline, Emeraldine and Leucoemeraldine (Fig. 6). They could be present either in their protonated (salt) or deprotonated (base) state. For a practical standpoint, the most useful form of PANI is Emeraldine because its preparation is straight forward, and it can be easily and reversibly switched from the insulating emeraldine base (EB) to the conducting emeraldine salt (ES) state, by protonation with an acid such as HCl (aq). The ES, in turn, can be dedoped/deprotonted with a base (NH_3) back to the insulating EB (Fig. 7).

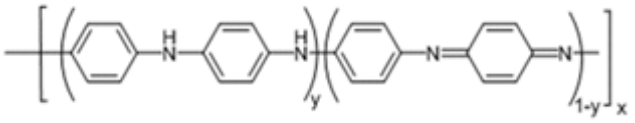

Figure 6. Base forms of Polyaniline: a) Pernigraniline (PB), y =0 b) Emeraldine (EB), y = 0.5 and c) Leucoemeraldine (LB), y =1. x is the number of repeat units

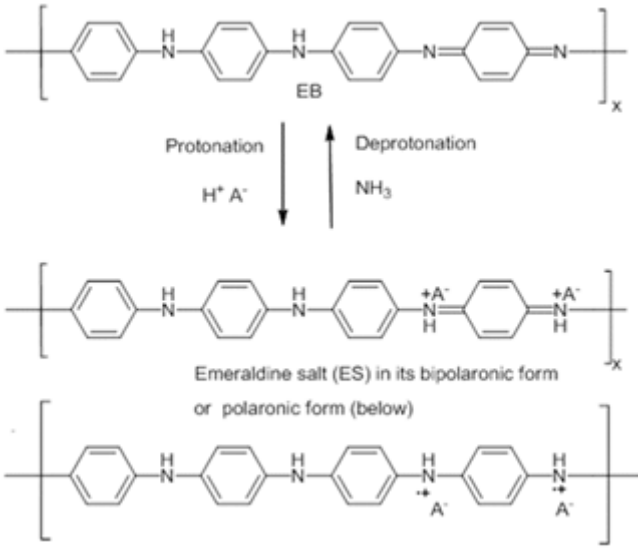

Figure 7. Process of protonation/doping of EB to form ES and deprotonation/dedoping of ES to form EB

Owing to PANI good conductivity, environmental stability and redox activity, their potential widespread applications as anti-corrosion agents, supercapacitors, LED, batteries, solar cells, anti-corrosion, chemical/ biochemical sensors, and electrochromic devices have been reported [11]. The past decades have witnessed a flurry of research aimed at the fabrication of nanocomposites of PANI as they offer higher aspect ratio useful in, e.g., biomedical applications [12]. In addition, the components of the nanohybrids could exhibit synergistic effect resulting in much better overall

properties than those of each individual component [13], [14]. PANI-Ag composites are often prepared in water in a single or double steps with $AgNO_3$ as the oxidizing agent. The single step/in-situ decoration of PANI could require weeks or months of polymerization time [15] because Ag^+ reduction potential (0.80V vs SHE) is much lower than that of the commonly used ammonium peroxysulfate (APS) whose reduction potential is 2.01 V vs SHE. Nevertheless, there are recent reports describing methods to improve the slow kinetics via, e.g., the use an initiator such as p-phenylenediamine [16], ultrasound and Gamma-radiation [17] or UV light [18].

The two-step/electrodeless procedure is a faster post polymerization decoration of EB with $AgNO_3$ (aq) which has been shown, in one instance, to yield higher conductivity for the composites [19].

In this study, we found that the dimer is insoluble in water, it is, however, soluble in polar solvents such as NMP or DMSO. In addition, the dimer exhibits redox activity at room temperature as shown above via cyclic voltammetry (Fig. 5). And at high temperature the dimer can be reduced by the DNBP ligand through its N-atom by charge transfer to the Ag(I), thereby producing metallic silver during melting (Fig. 5, inset). The dimer, therefore, is a good candidate for the decoration of PANI. Of interest to point out is the fact that the dimer is an organometallic compound; such reagents, to our knowledge, have not been used as a silver source to coat PANI after polymerization.

5. Results and Discussion

A series of silver decoration experiments of PANI with the dimer was conducted with EB either in solid state at high temperature or in NMP at ambient temperature. Assuming the reduction of Ag(I) to Ag metal is quantitative, the theorical mass % Ag in the final composites are 3%, 6% and 12%.

5.1. SEM Surface Analyses of PANI-Ag Composites

The decoration of PANI with metallic silver is conspicuous as revealed by SEM analyses. For example, Fig. 8a of a sample of EB-Ag (3%), (obtained under the stirred condition with NMP as solvent) shows the presence of unevenly dispersed metal clusters whose individual (semi) spherical metal particles are less than 100nm in diameters (Fig. 8b). They are coated onto the EB nanofibers of <100 nm in diameters. Semi quantitative elemental determination via EDS confirms the presence silver (Fig. 8c) when a larger size cluster (black dot on Fig. 8d) was analyzed. When a sample of EB-Ag was doped with 1M HCl, the resulting ES-Ag (3%) has metallic particles with sizes similar to those of the previously described dedoped EB counterparts (Fig. 8e). However, when the experiments were conducted with higher amounts of dimers, the as-produced PANI-Ag cluster morphology departs drastically from the above-described semi spherical structure, regardless of the experimental protocol used. The deposited Ag(s) exhibit various shapes and sizes with dimensions ranging from nano- to micrometer(s). For example, Fig. 8f displays an EB-Ag(6%) sample prepared in NMP at room temperature. The pebble like Ag(s) aggregates in Fig. 8g belongs to a sample of EB-Ag (6%) produced under thermal/solventless condition. And Fig. 8h features larger crystallites of an ES-Ag (12%) composite prepared in NMP solvent at room temperature.

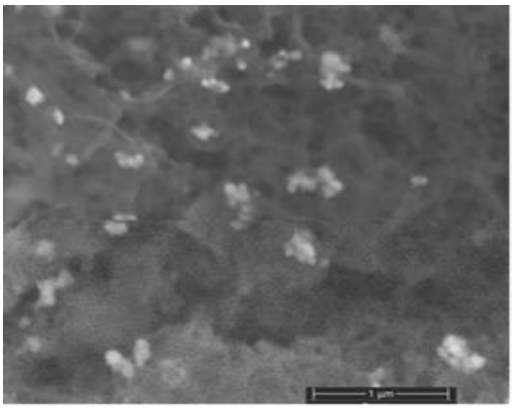

Figure 8a. EB-Ag (3%) composite isolated from NMP as solvent at room temperature (scale bar: 1μm)

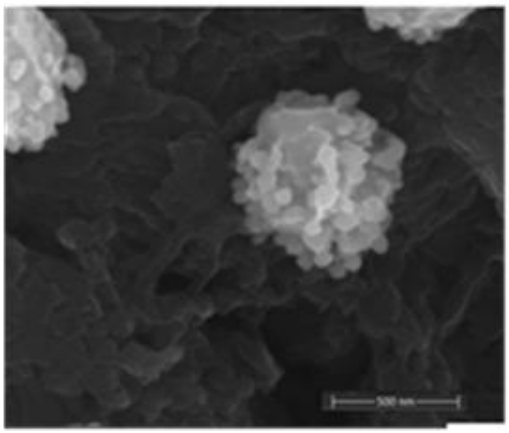

Figure 8b. EB- Ag (3%) composite showing a semi spherical Ag cluster composed of metallic particles of <100 nm in diameters (scale bar: 500 nm)

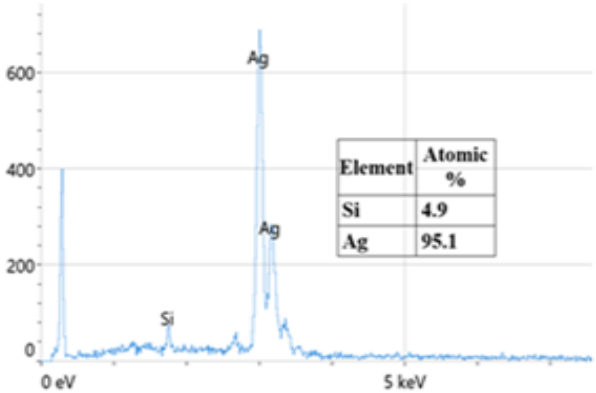

Figure 8c. EDS of an EB-Ag omposite confirming metallic silver deposited on EB. The presence of Si is from the silicon wafer used as substrate onto which the EB-Ag is deposited

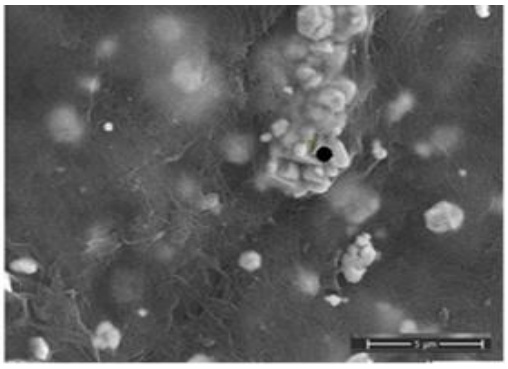

Figure 8d. EB- Ag (3%) composite with a large Ag cluster (scale bar: 1 μm)

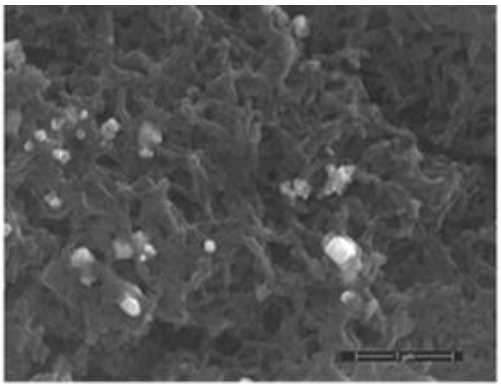

Figure 8e. ES-Ag (3%) composite with Ag deposited on nanofibers of PANI prepared from thermal/solventless condition (scale bar: 1μm)

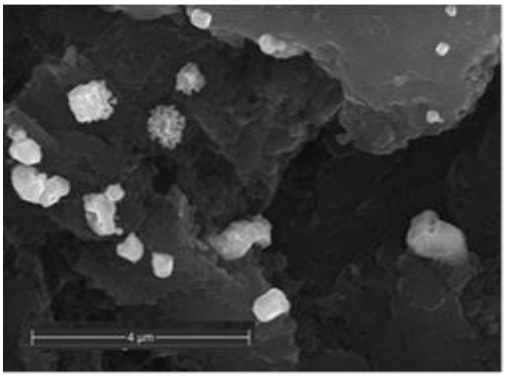

Figure 8f. EB-Ag (6%) composite isolated from NMP as solvent at room temperature (scale bar: 4 μm)

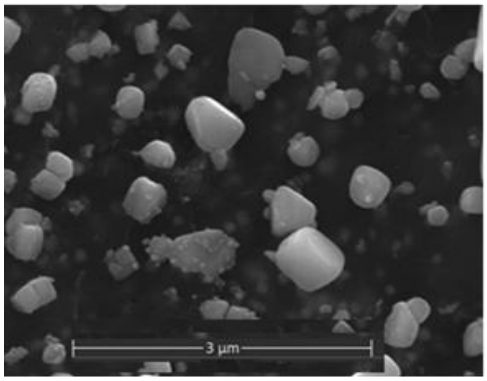

Figure 8g. EB-Ag (6%) composite prepared under solventless/thermal condition (scale bar: 3 μm)

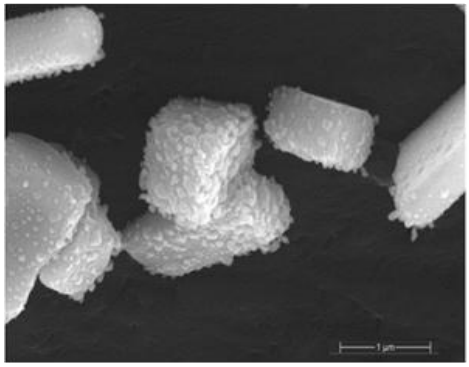

Figure 8h. ES-Ag (12%) composite prepared in NMP/room temperature (scale bar: 1 μm)

As mentioned above, the use (let alone the mechanism) of an organosilver as a metal source in post-polymerization decoration of PANI has not been reported. The deposition of metallic silver onto the PANI matrix could involve a preliminary step in which the dimer dissolves in the polar NMP solvent, releasing two monomers. This seems to be supported by the mass spectrometry (MS) data as only the monomer ion peak, but not that of the dimer, was observed when the polar DMSO was used to dissolve the analyte (unless the dimer ion peak quickly decomposes under the MS high energy condition). This dissolution step could be followed by a ligand exchange, involving the N atoms of the monomer and those of EB. Then Charge transfer from EB to the silver ion takes place, resulting in the formation of (semi) circular seeds onto which additional metal are deposited. The mechanism of Ag deposition on EB under the thermal/solventless condition most likely takes a different path. We note that when the pure dimer undergoes melting, a yellow brownish liquid melt is formed first. This preliminary step most likely involves the collapse of the weak H-bonds. And at slightly higher temperatures, reduction of Ag (I) occurs resulting in the formation of lustrous metallic beads (Fig. 5, inset). Such phenomenon may happen in this work, i.e., the decoration process may not involve EB unless the above-described sequential steps of rapid ligand exchange in the molten medium and then charge transfer from EB nitrogens to the metal ion takes place. It is likely that the initial metal seeds formed in both experimental procedures ((heat or room temperature) had served as templates for additional metal growth to produce larger structures as evidenced in Fig. 8g and 8h which clearly show the presence of grainy particles growing on the chunky or elongated (semi)micron-sized structures. These large silver aggregates may stem from the inhomogeneity of the reaction medium where the reagents are not well dispersed. In this medium, random nucleation and seed migration might take place resulting in the formation of structurally ill-defined but thermodynamically stable crystallites.

5.2. UV-VIS Analyses of the PANI-Ag Composites

The UV-Vis spectra of the parent/undecorated EB (Fig 9)

displays the two typical absorptions bands: one at 328 nm which is assigned to the π-π * transition in the benzenoid ring, and the other at 635 nm which is associated with the excitation transition ("n-π*") in the quinoid rings [20].

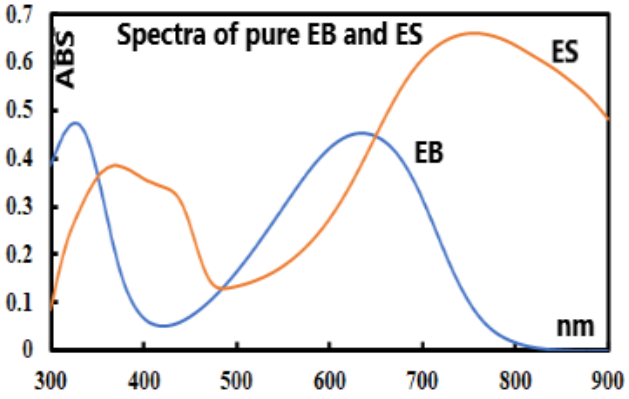

Figure 9. UV-vis spectra of the undecorated parent EB and ES

Representative spectra of EB-Ag composites are found in Fig 10. They resemble the above undecorated EB spectrum except their ("π -π*") transitions are slightly red shifted and their ("n -π*") are blue shifted (Table 1). The blue shift could indicate partial oxidation of EB by the silver ion to pernigraniline.

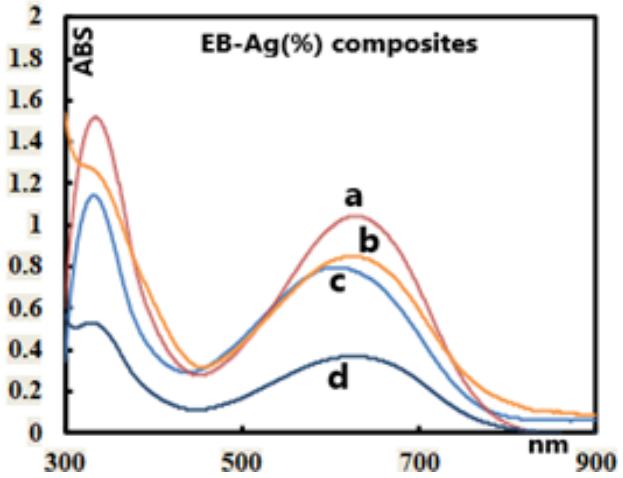

Figure 10. UV-vis spectra of representative EB-Ag (%) composites/experimental cconditions: a: (6%) /heat and solventless; b: (6%) /room temperature/NMP; c: (3%)/heat and solventless; d: (3%)/room temperature/NMP

The undecorated ES spectrum of the parent conducting PANI (Fig. 9) displays the three typical absorptions at: 356nm (π-π* transition), the polaron-π* (p-π*) transition at 440 nm which is characteristic of a protonated/doped PANI state and the π-polaron (π-p) transition at 834 nm, commonly called "free carrier tail, which is another characteristic of a conducting PANI [21]. Similarly, the representative spectra of the decorated ES-Ag (Fig 11) show the above-mentioned parent ES transitions with their specific wavelengths given in Table 2. With respect to the π--->π* transition of the parent ES, those belonging to the composites are red shifted.

Table 1. UV-Vis characteristics of representative EB-Ag composites

EB-Ag %	Experimental condition	π --->π * (nm)	n---> π * (nm)	Plot in Fig.10
3%	thermal/solvent less	335	606	c
6%	thermal/solvent less	336	629	a
3%	25℃/NMP	333	626	d
6%	25℃/NMP	336	625	b

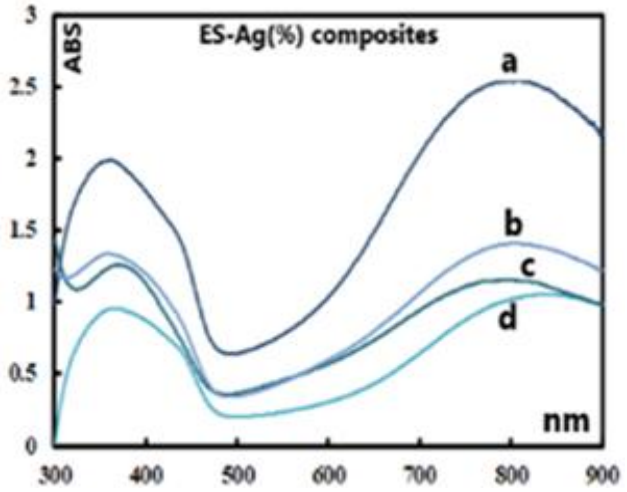

Figure 11. UV-vis spectra of representative ES-Ag (%) composites/experimental cconditions: a: (3%) /heat and solventless; b: (3%) /room temperature/NMP; c: (6%) room temperature/NMP; d: (6%)/heat and solventless

Table 2. UV-Vis characteristics of representative ES-Ag composites

ES-Ag %	Experimental condition	π --->π* (nm)	p- π* (nm)	π-p (nm)	Plot in Fig.11
3%	thermal/no solvent	364	438	810	a
6%	thermal/no solvent	368	440	844	d
3%	25℃/NMP	363	436	808	b
6%	25℃/NMP	371	439	796	c

5.3. Determination of Band Gap

The electric conductivity of the intrinsically conducting polymers are obtained via the four-probe technique and their band gaps (BG) are determined using the Tauc equation: $\alpha h\nu = A(h\nu - E_g)^n$ where α is the absorbance, hv the incident photon energy, A is the BG tailing coefficient (a constant nearly independent of the photon energy parameter) and E_g the optical BG. The exponent n can take values of 0.5, 1.5, 2 or higher depending on the nature of the transitions, i.e., whether they are allowed or forbidden and direct or indirect. If the transition is allowed and direct, the n value is 0.5. An n value of 1.5 indicates a direct but forbidden transition whereas a value of 2 is associated with an allowed but indirect transition [22]. The photon energy hv (in ev) can be

expressed as a function of the incident light wavelength and written as 1240/λ, with λ in nm. In this study, the energy (1240/λ) is plotted against $(\alpha hv)^{0.5}$ which provided a straight line fit implying a direct and allowed transition. The BG is obtained by extrapolating the straight-line portion of the graph onto the hv axis where α=0. Representative plots for the BG determination are given in Fig. 12 and 13.

Table 3 provides the BG of the composites and their electrical conductivities. The corresponding values of the undecorated/parent ES are 0.51ev (inset of Fig. 12) and 0.18 S/cm, respectively. The latter is close to that of the reported value (0.21S/cm) for a sample prepared under conventional protocol with APS as the oxidizing agent [23]. It is worth noting that all measured BG fall in between 2 and 3 ev which is the common range of silver decorated PANI [22] or undecorated ES [24]. It should be pointed out that the BG are approximate since they are derived from UV-Vis analyses which take only into account the NMP soluble portion of the polymers whereas the conductivities are derived from the original solids and thus, should reflect better the properties of the as-prepared samples. The data indicate that the conductivities of the composites prepared from both procedures (heat or room temperature) increase with the mass percent silver in the composites. They are higher than that of a) the above mentioned undecorated parent ES, b) a PANI-nanoAg composite (0.2 S/cm) prepared from polymerizing aniline with APS as co-oxidant in a solution containing $AgNO_3$ having an initial concentration of 0.02M [25], c) an ES-Ag ($1.5X10^{-3}$ s/cm) obtained from grinding solid $AgNO_3$ with aniline hydrochloride [23] or d) derivatives of PANI such as poly (2,5-dimethoxyaniline)-Ag nanocomposites (10^{-4}-10^{-2} S/cm) [26]. Nevertheless, the conductivities recorded in this study cannot rival the electrical property of a) PANI-nanoAg (100 S/cm) composite prepared in a two-step sequence in which a preliminary prepared PANI-Ag is immersed into a solution of $AgNO_3$ (aq) for additional metal decoration [19], b) PANI-Ag complexes with high content of silver: 38.48% (535.2 S/cm) [27] or an ES with close to 80% Ag (2250 S/cm) [28]. Moreover, the enhancement in conductivity, observed in this study, through the incorporation of silver onto the pure ES is rather modest. This finding corroborates with the observation of Stejskal et al. who demonstrated that ES (not the metal) is the major contributor to the overall conductivity of PANI-silver composites [19]. With respect to most reported PANI-Ag composites where the Ag particles are nanosized and their shapes are quite homogeneous [13,25,26,27], those found in this work vary from nano to micrometer in dimensions and they adopt different structures depending on the metal loading. This difference in morphology along with the uneven distribution of the metallic particles in the PANI host contributed to the observed conductivity. Improving the electrical properties of PANI-metal composites remains challenging and it is the subject of continued research. It requires the control of multiples variables such as a) the relative ratio of metal/polymer which affects the overall density of the composite, and b) the presence of oligomers around the metal which influences the conductivity and/or potential percolation at the interface between the metal and the polymer [19], [29].

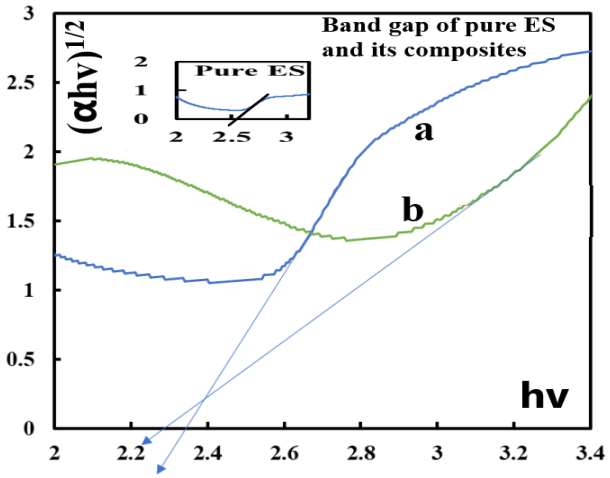

Figure 12. Tauc plots for the determination of band gap values of pure ES (inset) and ES-Ag (%) composites prepared at room temperature in NMP a: (3%) ; b: (6%)

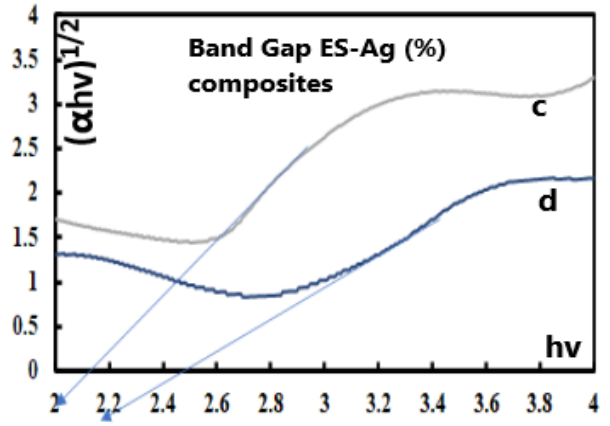

Figure 13. Tauc plots for the determination of band gap values of ES-Ag (%) composites prepared under solventless condition at high temperature: c: (6%); d: (3%)

Table 3. Band gaps and conductivities of ES-Ag composites

Percent Ag in composite	Experimental condition	Band gap (ev)	conductivity (S/cm)	Plot in Fig. 12 and 13
3%	thermal/no solvent	2.42	0.33	d
6%	thermal/no solvent	2.18	0.71	c
12%	thermal/no solvent	2.07	0.85	-
3%	25℃/NMP	2.36	0.39	a
6%	25℃/NMP	2.28	0.48	b
12%	25℃/NMP	2.20	0.66	-

5.4. IR Analyses

Representative IR spectra of EB, EB-Ag and ES-Ag are

shown in Fig. 14, 15 and 16. Their vibrations (cm^{-1}) are as follows:

EB: 3448.27, 1585.60, 1491.69, 1409.77, 1378.10, 1298.30, 1267.13, 1159.20, 1132.54, 954.37, 854.37, 827.40 695.72, 499.52.

EB-Ag: 3446.15, 1587.22, 1495.32, 1384.01, 1323.95, 1286.01, 1133.50, 1123.73, 796.93, 701.03, 496.02.

ES-Ag: 3447.43, 1577.90, 1491.80, 1383.41, 1298.02, 1139.07, 821.38, 797.94, 697.65, 599.30, 503.86.

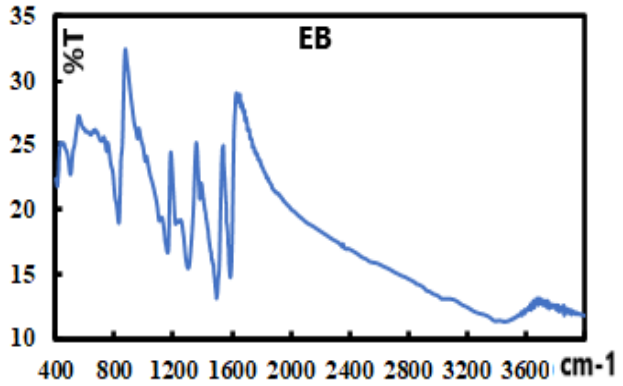

Figure 14. IR spectrum of pure EB

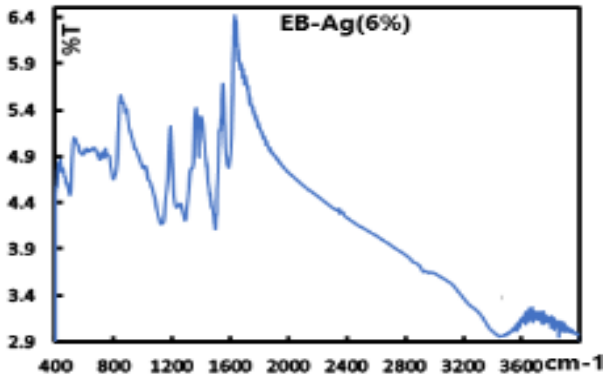

Figure 15. IR spectrum of EB-Ag (6%) prepared from thermal/solventless condition

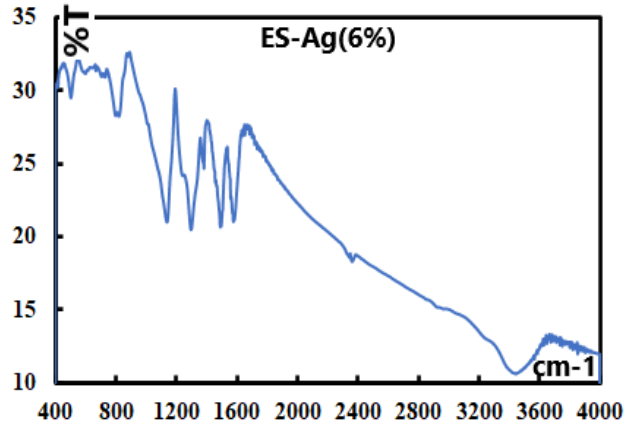

Figure 16. IR spectrum of ES-Ag (6%) prepared in thermal/soventless condition by doping the corresponding EB-Ag(6%) with 1M HCl

The FT-IR stretching modes of the parent EB, its decorated dedoped (EB-Ag) and doped (ES-Ag) polymers are given in Table 4. They show the presence of PANI through their typical vibrations around the following ranges: a) 3450-3445 cm^{-1} (N-H stretching) [17], [30], b) 1590-1575 cm^{-1} (C=N stretching of quinoid ring) [17], [30], c) 1496-1490 cm^{-1} (C=C stretching of benzenoid ring [17], [30], d) around 1300 cm^{-1} (C-N stretching of benzenoid ring) [17], [22], [31]. The identifiable bending modes of these polymer/composites are given in Table 5. The broad band of ES-Ag at 1139.07 cm^{-1} is shifted to higher wavenumber compared to the corresponding vibration of the dedoped EB or EB-Ag. This band has been assigned by Camilo et al. [32] to the in- plane C–H bending vibrations in the quinoid ring of a doped ES-Ag nanocomposite. A similar band located at 1142 cm^{-1} of an ES-nanoAg sample has also been described by Azevedo et al. [17]. The aromatic C-H out of plane bending mode of EB is at 827 cm^{-1} [30]. The corresponding vibration of its silver decorated doped or dedoped counterparts have lower wavenumbers. The C-C deformation modes for the benzenoid ring are close to 700 cm^{-1} [33] and the C-N-C torsion vibrations are located around 500 cm^{-1} [34].

Table 4. Specific IR stretchings of EB, its doped and dedoped Ag composites

EB and its composites	N-H stretch	N=Q=N stretch (Q=Quinoid ring)	N=B=N stretch (B=Benzenoid ring)	C-N stretch of B-ring
EB	3448.27	1585.60	1491.69	1298.30
EB-Ag	3446.15	1587.22	1495.32	1323.95
ES-Ag	3447.43	1577.90	1491.80	1298.02

Table 5. Specific IR bendings of EB, its doped and dedoped Ag composites

Polymer/ composites	Ar-C-N-C bending	C-H bending	C-C ring deformation	C-N-C torsion
EB	1132.54	827.40	695.72	499.52
EB-Ag	1133.50	796.93	701.03	496.02
ES-Ag	1139.07	821.38	697.65	503.86

6. Conclusions

We have synthesized and characterized the dimer of (Nitrato-κ^2 O, O′) bis (2-(2,4-dinitrobenzyl) pyridine κ-N) silver (I). Owing to the redox properties of this organosilver compound, we showed that it can be used to decorate polyanilines under thermal/solventless condition or at room temperature in NMP solvent. Both procedures yield silver decorated PANI which were characterized by UV-Vis, IR spectroscopy and SEM. Surface analyses of the composites via SE micographs revealed that at low silver concentration, the metal is deposited on the PANI matrix as (semi) spherical clusters composed of particles with average diameters in the nanometer range. At higher concentrations, the particles tend to aggregate forming larger structures of various shapes with dimensions ranging from nano- to micrometers. It is found

that the conductivity of the composites increases with increasing loading of silver and is moderately above that of the undecorated PANI.

ACKNOWLEDGEMENTS

The authors are grateful to the Foundation of the University of Science and Arts of Oklahoma for its partial financial contribution to the project through the Gladys Anderson Emerson research fund. They acknowledge the help and thank Dr. Douglass Powell of the University of Oklahoma for collecting X-Ray crystallographic data and for the determination of the dimer structure. Dr. Powell thanks the National Science Foundation for a grant (CHE-1726630) and funds from the University of Oklahoma for the purchase of the X-ray diffractometer and computers.

REFERENCES

[1] A. Corval, K. Kuldova, Y. Eichen, Z. Pikramenou, J. M. Lehn, H. P. Trommsdorff., 1996, Photochromism and thermochromism driven by intramolecular proton transfer in dinitrobenzylpyridine compounds, J. Phys. Chem., 100, 19315-19320.

[2] H. Sixl, R.Warta., 1985, Reaction mechanism of photochromic 2-(2', 4'-dinitrobenzyl) pyridine (DNP) single crystals, Chem. Phys. 94 (1-2), 147-155.

[3] V. Arcisauskaite, J. Kongsted, T. Hansen, K. V. Mikkelsen., 2009, Charge transfer excitation energies in pyridine-silver complexes studied by QM/MM method, Chem. Phys. Lett., 470 (4-6), 285-288.

[4] G. A. Bowmaker, K.C. Lim, B. W. Skelton, D. Sukarianingsingsih, A. White., 2005, Syntheses, structures, and vibrational spectroscopy of some 1:2 and 1:3 adducts of silver (I) oxyanion salts with pyridine and piperidine bases containing non coordinating 2(,6)-substituents, Inorg. Chim. Acta, 358 (14), 4342-4370.

[5] K. Self, K. N. Trueblood., 1968, The crystal structure of 2-(2',4'-dinitrobenyzyl) pyridine, Acta Cryst., B24, 1406-1415.

[6] N. M. Zaczek, W.D. Levy, M. L. Jordan, J. A. Niemyer., 1982, Synthesis of photochromic 2-(2,4-dinitrobenzyl) pyridine, J. Chem. Ed., 59 (8), 705.

[7] M. C. McGoran, K. Hintz, K. Hoffman, R. Lovin., 2006, Enhancement on the photochromism of 2-(2,4-dinitrobenzyl) pyridine: molecular modeling, NMR, photo- and solvent bleaching, J. Chem. Ed., 83 (6), 923-926.

[8] A. A. Sayed, M.K., Dinesan., 1991, Review: Polyaniline, A novel polymeric material, Talenta, 38 (8), 815-837.

[9] F. Roussel, R. Chan-Yu-King, M. Kuriakose, M. Depriester, A. Hadj-Sahraoui, C. Gors, A. Addad, J-F. Brun., 2015, Electrical and thermal transport properties of polyaniine / silver composites and their use as thermoelectric materials, Synth. Met., 199, 196-204.

[10] X. Zhang, W. J. Goux, S. K. Manohar., 2004, Synthesis of polyaniline nanofibers by "nanofiber seeding", J. Am. Chem. Soc., 126 (14), 4502-4503.

[11] R. Kumar, S. Singh, B. C. Yadav., 2015, Conducting polymers: synthesis, properties and applications, Int. Adv.. Res. J. Sci. Eng. Technol., 2 (11), 110-124.

[12] E. N. Zare, P.Makvandi, B. Ashtari, F. Rossi, A. Motahari, G. Perale., 2020, Progress in conductive polyaniline-based nano-composites for biomedical applications: a review, J. Med. Chem., 63 (1), 1-22.

[13] Q. Jia, S. Shan, L. Jiang, Y. Wang, D. Li., 2012, Synergistic antimicrobial effects of polyaniline combined silver nanoparticles, J. Appl. Polym. Sci., 125 (5), 3560-3566.

[14] Z. Pei, L. Ding, M. Lu, Z. Fan, S. Weng, J. Hu, P. Liu., 2014, Synergistic effect in polyaniline-hybrid defective ZnO with enhanced photocatalytic activity and stability, J. Phys. Chem. C., 118 (18), 9570-9577.

[15] N. V. Blinova, J. Stejskal, M. Trchova, I. Sapurina, G. Ciric-Marjanovic., 2009, The Oxidation of aniline with silver nitrate to polyaniline-silver composites, 50, 50-56.

[16] P. Bober, J. Stejskal, M. Trchová, J. Prokes, I. Sapurina., 2010, Oxidation of aniline with silver nitrate accelerated by p-phenylenediamine: a new route to conducting composites, Macromolecules, 43 (24), 10406-10413.

[17] W. M. de Azevedo, R. A. de Barros, E. F. da Silva Jr., 2008, Conducting polymer preparation under extreme or non-classical conditions, J. Mater. Sci., 43, 1400-1405.

[18] Z. Li, Y. Li, W. Lin, F. Zheng, J. Laven., 2016, Polyaniline/silver nanocomposites synthesized via UV-Vis assisted aniline polymerization with a reverse microemulsion system, Polym. Compos. 37, 1064-1071.

[19] P. Bober, J. Stejskal, M. Trchová, J. Prokes., 2014, In-situ prepared polyaniline–silver composites: single- and two-step strategies, Electrochim. Acta, 122, 259-266.

[20] K. Tzou, R.V. Gregory., 1993, A method to prepare polyaniline salt solutions-in situ doping of Pani base with organic dopants in polar solvents, Synth. Met., 53 (3), 365-377.

[21] A. G. MacDiarmid, A. J. Epstein, 1994, The concept of secondary doping as applied to polyaniline, Synth. Met., 65 (2-3), 103-116.

[22] S. M. Reda, S. M. Al-Ghannam, 2012, Synthesis and electrical properties of polyaniline composite with silver nanoparticles, Adv. Mater. Phys. Chem., 2, 75-81.

[23] I. Sedenkova, E. N. Konyushenko, J. Stejskal, M. Trchova, J. Prokes, 2011, Solid-state oxidation of aniline hydrochloride with various oxidants, Synth. Met., 161 (13-14), 1353-1360.

[24] N. Karaoglan, C. Bindal., 2018, Synthesis and optical characterization of benzene sulfonic acid doped polyaniline, Eng. Sci. Technol. Int. J., 21 (6), 1152-1158.

[25] S. K. Pillalamarri, F. D. Blum, A. T. Tokuhiro, M. F. Bertino., 2005, One pot synthesis of polyniline-metal nanocomposites, Chem. Mater., 17, 5941-5944.

[26] G. M. Neelgund, E. Hrehorova, M. Joyce, V. Bliznyuk., 2008, Synthesis and characterization of polyaniline derivative

and silver nanoparticle composites, Polym. Int., 57 (10), 1083-1089.

[27] L. Xia, C. Zhao, X. Yan, Z. Wu., 2013, High conductivity of polyaniline-silver synthesized in situ by additional reductant, J. Appl. Polym. Sci., 130 (1), 394-398.

[28] N. V. Blinova, J. Stejskal, M. Trchova, I. Sapurina, G. Ciric-Marjanovic., 2009, The oxidation of aniline with silver nitrate to polyaniline-silver composites, Polymer, 50 (1), 50-56.

[29] M. Trchová, Z. Moravkova, J. Dybal, J. Stejskal., 2014, Detection of aniline oligomers on polyaniline-gold using resonance raman scattering, ACS Appl. Mater. Inter., 6(2), 942-950.

[30] W. Shao, R. Jamal, F. Xu, A. Ubul, T. Abdiryim., 2012, The effect of a small amount of water on the structure and electrochemical properties of solid-state synthesized polyaniline, 5, 1811-1825.

[31] S. Golba, , M. Popczyk, S. Miga, J. J. Suliga , M. Zubko, J. Kubisztal, K. Balin., 2020, Impact of acidity profile on nascent polyaniline in the modified rapid mixing process—material electrical conductivity and morphological study, Mater., 13, 5108-5123.

[32] C. M. Correa, R. Faez, M. A. Bizeto, F. F. Camilo., 2012, One pot synthesis of a polyaniline-silver nanocomposite prepared in ionic liquid, RSC. Adv., 2, 3088-3093.

[33] A. Olad, S. Behboudi, A. A. Entezami., 2012, Preparation, characterization and photocatalytic activity of TiO2/ polyaniline core-shell nanocomposite, Bull. Mater. Sci., 35 (5), 801-809.

[34] C. Dhivya, S. A. A. Vandarkuzhali, N. Radha., 2019, Antimicrobial activities of nanostructured polyanilines doped with aromatic nitro compounds, Arab. J. Chem., 12 (8), 3785-3798.